Hybrid SMF–FSO–VLC long-reach wheel basics PON achieving 2 Tbps via integrated OFDM–OCDMA methodology

VIVEK ARYA[1,*], SHIPRA SHUKLA[2], TAPSI NAGPAL[3], RIYAZ BASHA MANDIYAM[4], SAMANA VINAYA KUMAR[5], SUBODH BANSAL[6]
[1]*Phonics University, Roorkee-247667, Uttarakhand, India*
[2]*School of Computing Science, CSE Galgotias University, Greater Noida, U.P., India*
[3]*IT Department, New Delhi Institute of Management, New Delhi, India*
[4]*King Saud University - (Common First year), Riyadh, Saudi Arabia*
[5]*Department of Electronics and Communication Engineering, Aditya University, Surampalem, Andhra Pradesh, India*
[6]*Department of ECE, UIE Chandigarh University, Mohali-140413, Punjab, India*

This work introduces an integrated single-mode fiber, free space and visible light communication links in next-generation passive optical network (PON) enabled orthogonal frequency division multiplexing as well as optical code division multiplexing. The results reveal reliable fiber, FSO and VLC range of 100 km, 2800 m and 20 m, respectively, at an aggregate data rate of 2Tbpsunder critical climate and turbulence. Also, it offers acceptable power penalties of 1-2 dB with maximum power budgets of -26 dBm and -39 dBm receiver sensitivity with 12 dB insertion loss. The comparative literature underscores its advantage over other designs in terms of code implementation and overall design.

(Received August 18, 2025; accepted April 8, 2026)

Keywords: 2D-MFRS, POLAN, PON, VLC, FSO

1. Introduction

Despite modern technological progresses, concerning with disasters debris fatiguing, especially if they exactly bother human health, such as COVID-19 pandemic. Owing to the insufficient willingness, the hospitals or healthcare centers could not deal with several patients. After the declaration of pandemic several people were incapable to receive medical assistance worldwide because of shortage of access to essential health services. This pandemic demonstrated that an increase in the number of patients, inadequate medical services, late response and failure to prevent the infection caused the healthcare system to fail [1]. Furthermore, this failure has made people conscious of the advantages of intelligent healthcare system for disaster preparedness. Therefore, it is incredibly crucial to develop the intelligent healthcare system. The steps towards intelligent healthcare systems connected with several smart healthcare devices, medical apparatuses, hospitals and patients/doctors demands high bandwidth, high transmission rate, low latency, ultra-reliability, low cost and low power communication [1,2].

Furthermore, among the several advanced passive optical network PON techs, hybrid wavelength division multiplexing and optical code division multiplexing (WDM-OCDM) methods are the most favorable. OCDM signals may be superimposed over WDM networks to grow the data capacity as well as confidentiality over the wider transmission range, as per several studies on hybrid WDM-OCDM PON. In [3], hybrid WDM-OCDM PON at symmetric 1.25 Gbps transmission rate over 22 km fiber range has been demonstrated. Also, in [4], an integrated WDM-OCDM PON at 20 km fiber link at 80 Gbps throughput has been reported. In another work [5], an experimental demonstration of hybrid WDM-OCDM PON at 1.25 Gbps traffic rate over 23 km range has been presented.

Meanwhile, optical fiber transmissions possess reliability issues and nonlinear effects owing to fiber fault during laying or digging of new network infrastructure. For this, hybrid fiber and free space optics (FSO) link dominance the advantages of fiber and FSO links at moderate maintenance cost. However, in hybrid fiber-FSO communication, FSO performance is quite sensitive to atmospheric conditions and turbulence effects [6]. The combination of both fiber and FSO is becoming a favorite solution for allowing limited energy consumption, high speed, reliable, low maintenance, secured and cost-effective internet services. It provides better solutions against fiber breakage than conventional fiber as well as radio frequency communication [7]. Besides this, there may be certain service interruptions in FSO line of sight (LOS) path like birds, butterflies, moving objects etc. Recently, aPON-FSO system over 300 m FSO and 25 km fiber span at 10Gbps traffic rate has been demonstrated in [8]. To extend free-space range upto 1.4 km, a hybrid fiber-FSO system at 1 Gbps information rate over 20 km fiber is also reported in [9].

The proposed scheme provides least restoration time (7 ms) for the protection of the PON. In [10], a ring topology based WDM-PON has been realizedto analyze the design reliability as well as network scalibility. It is reportd that receeiver sensivity of -26 dBm can be obtained with ring topology supporting eight remote nodes (RNs). In [11], a ring-based PON architecture using asymemetric passive splitters has been experimental demonstrated. It is presented that demonstraed architecture can provide traffic full restoration if an optical line terminal (OLT) is failed in various services. In addition, a ring-tree toplogy based WDM system supporting 64 consumers at 60 Gbps has been reported in [12]. In another work [13], an integrated ring-star based dense WDM architecture supporting 128 users over 150 km transmision distance at 15 Gbps throughput has been investigated. Moreover, a dual-ring basics hybrid fiber/FSO link in WDM system over 5 km range at 20 Gbsp traffic rate has been proposed.

1.1. Motivation

High-bandwidth, robust, high-speed, flexible, anytime-anywhere and low cost communication technology allows business and subscribes to access many resources and services, including e-commerce, education, entertainment, public security, healthcare scenario etc. [14]. OCDMA PON using orthogonal frequency division multiplexing (OFDM) modulation over integrated single mode fiber (SMF) and FSO-VLC links is more robust and fault tolerant than PON due to the self-healing capability of the wireless end. In the healthcare systems where fiber links are impractical or in rural areas that lacks fiber infrastructure, long range FSO and human friendly visible light communication (VLC) communication can be incorporated in such areas. In the rapidly expanding healthcare sector, there are still several problems and challenges that need to be resolved.

1.2. Contribution

In this work, a next-generation symmetric PON using integrated OFDM-OCDM system utilized wheel topology considering the impact of atmospheric scenario is investigated. Major contributions are as follows:

1) However, integrated PON/FSO/VLC designs have been studied over the past 15 years, but for next generation PON (NGPON) stage 3 employing all OCDMA, OFDM, WDM techniques for next-generation applications is reported first ever in this work.
2) The study explores a proactive protection architecture designed for hybrid optical wired–wireless networks to mitigate failures resulting from unforeseen disasters, particularly weather-related impairments like fog, rain, snow, and weak-to-strong turbulence.
3) To measure system performance in terms of insertion loss, receiver sensitivity, error rate, quality factor, gain, noise figure, receiver output and link noise.
4) The proposed design is validated by comparing its performance against existing approaches.

This work is structured as: Proposed architecture considering fiber, VLC, and FSO links disturbances is presented in Section 2. Mathematical analysis and evaluated results with discussion are shown in Section 3. Conclusion remarks with future scope are exhibited in Section 4.

2. Proposed design

Fig. 1 presents the wheel-hybrid PON/FSO/VLC healthcare system.

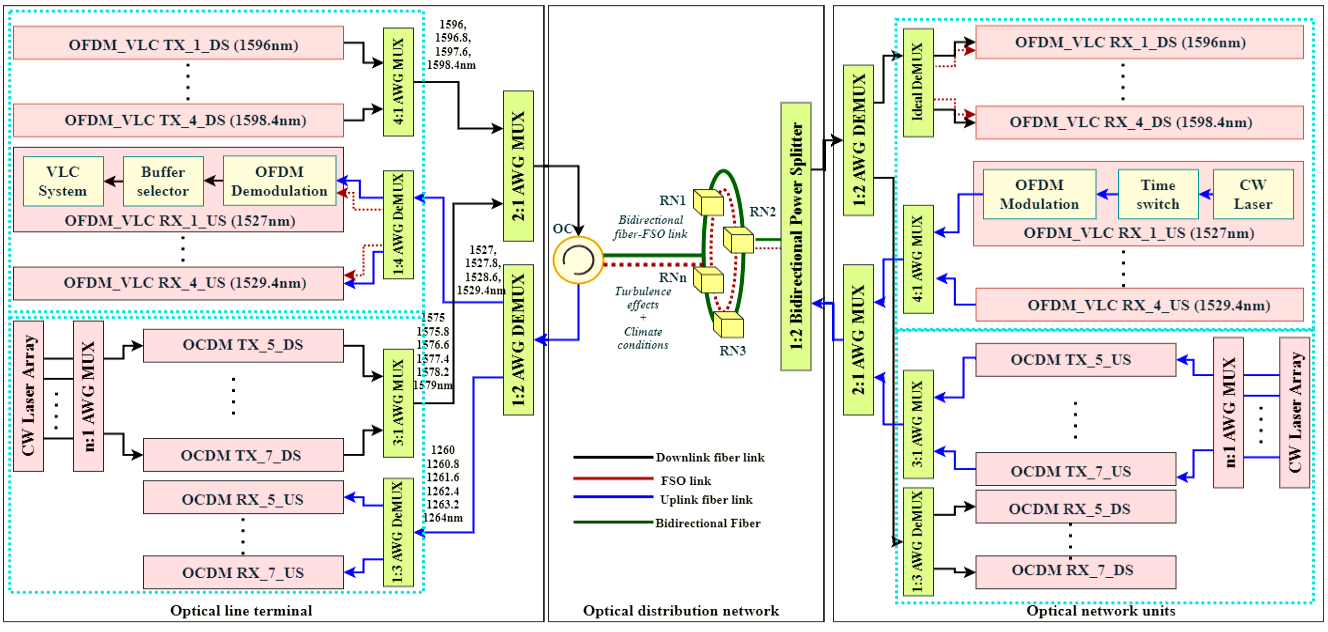

(a)

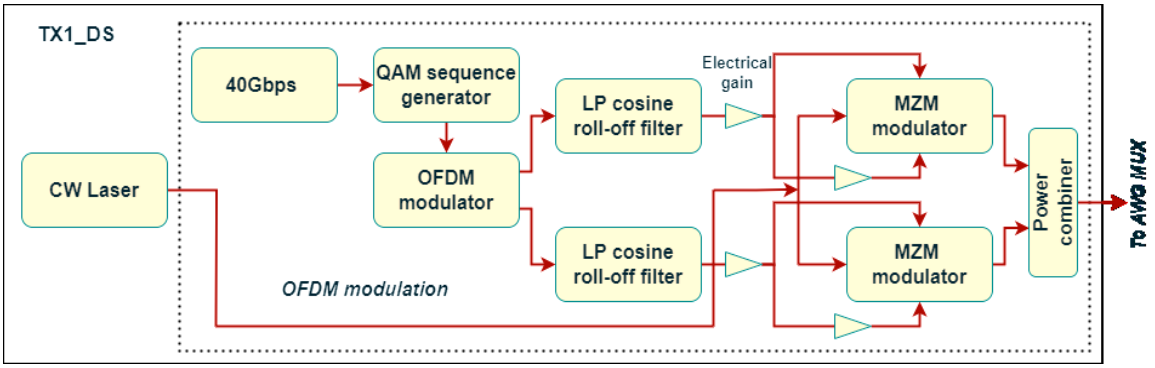
TX1_DS
40Gbps
QAM sequence generator
LP cosine roll-off filter
Electrical gain
MZM modulator
CW Laser
OFDM modulator
LP cosine roll-off filter
MZM modulator
Power combiner
To AWG MUX
OFDM modulation

(b)

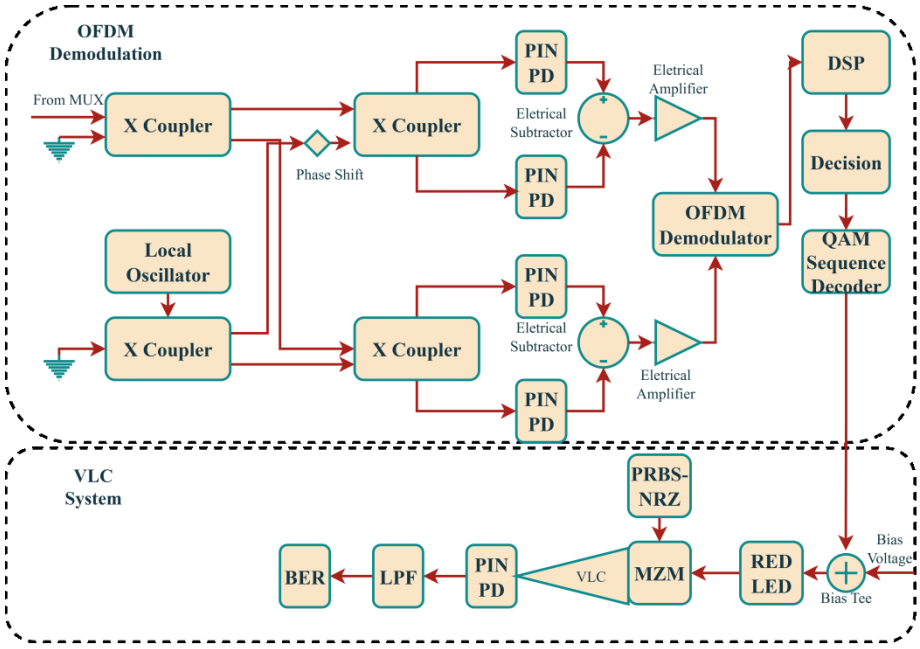
OFDM Demodulation
From MUX
X Coupler
X Coupler
PIN PD
Eletrical Amplifier
DSP
Eletrical Subtractor
Phase Shift
PIN PD
Decision
OFDM Demodulator
Local Oscillator
QAM Sequence Decoder
PIN PD
X Coupler
X Coupler
Eletrical Subtractor
Eletrical Amplifier
PIN PD
VLC System
PRBS-NRZ
Bias Voltage
BER
LPF
PIN PD
VLC
MZM
RED LED
Bias Tee

(c)

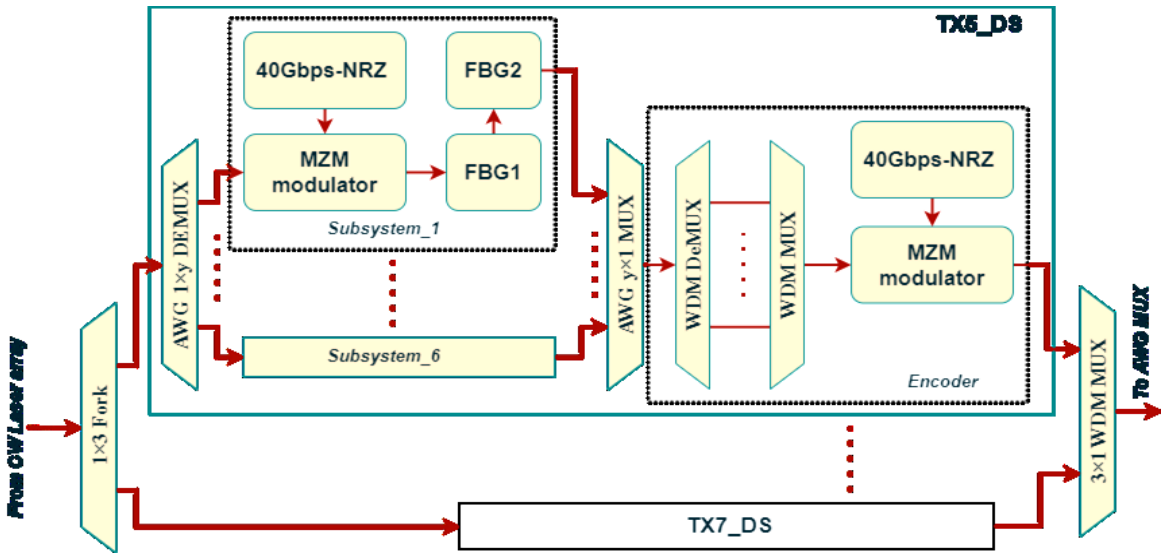
TX5_DS
40Gbps-NRZ
FBG2
MZM modulator
FBG1
Subsystem_1
AWG 1×y DEMUX
Subsystem_6
AWG y×1 MUX
WDM DeMUX
WDM MUX
40Gbps-NRZ
MZM modulator
Encoder
From CW Laser src
1×3 Fork
3×1 WDM MUX
To AWG MUX
TX7_DS

(d)

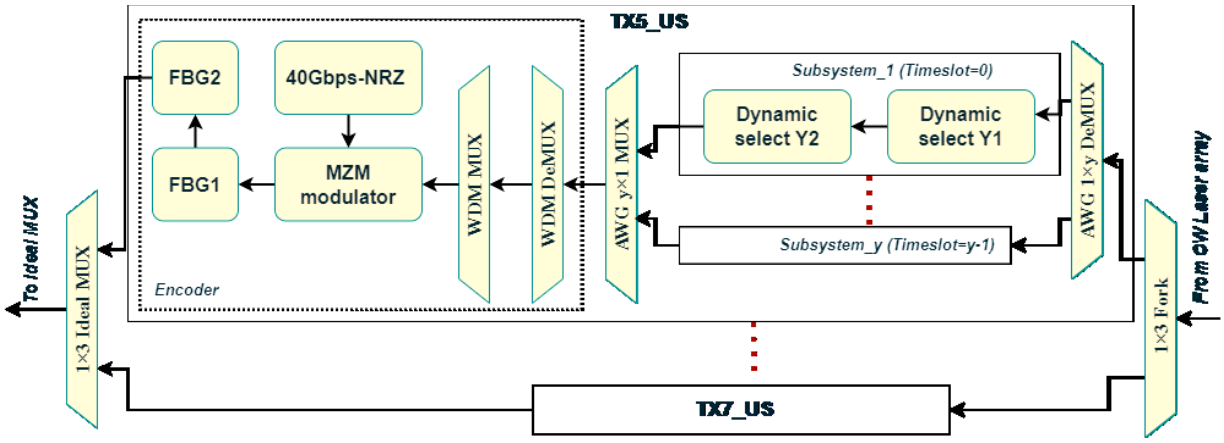

(e)

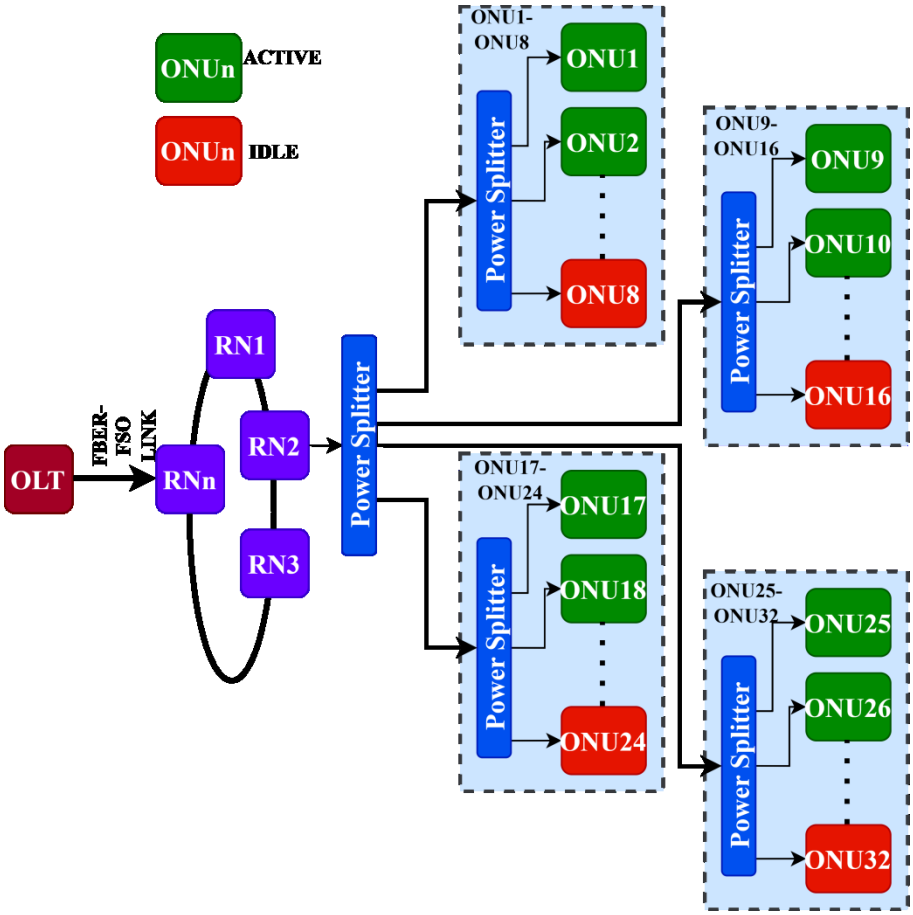

(f)

Fig. 1. (a) Architecture of proposed POLAN system using hybrid OFDM-OCDMA techniques; TWDM (b) DS Tx section, (c) DS Rx section; WDM-OCDMA (d) DS Tx, (e) US Tx, (f) schematic diagram of 20 ONUs per RN in the system (colour online)

The schematic plot of wheel-bidirectional PON system for healthcare scenario under uncertain environment conditions is shown in Fig. 1. The combination of an integrated time and wavelength division multiplexing (TWDM) OFDM PON/VLC system with modulation format of four level quadrature amplitude modulation (4-QAM) and hybrid WDM-OCDMA system using 2D-MFRS code is presented. As compared to higher order modulation formats 4-QAM tends to forward high bandwidth information (>100 Gbps) over optical link and offer best performance w.r.t. receiver sensitivity. The system is investigated over hybrid fiber, FSO and VLC links in both DS and US directions. The system is mainly designed for disaster preparedness in healthcare systems

considering fiber impairments, FSO turbulent and weather conditions. Here, the presence of FSO channel acts as a backup protection link in the outdoor region whenever the geographic regions are too difficult/unstable to realize fiber links because of presence of mountain, rocky ground, wider river and another environs factors. End users (patients or doctors) and devices are linked via a high-quality red LED based VLC communication link [15].

As shown in Fig. 1(a), at OLT, the downstream OFDM modulated signals and OCDM coded signals received from 4:1 array waveguide grading multiplexer (AWG MUX) and 3:1 AWG MUX respectively, is send to a 2:1 AWG MUX followed by a bidirectional optical circulator. Then, these signals are directed towards a full-duplex fiber-FSO link and multiple remote nodes (RNs) concerning channel impairments and atmospheric conditions in optical distribution network (ODN). For data reception from each RN, a 1:2 bidirectional splitter is used to split the signals into two segments i.e. downstream (DS) reception and upstream (US) transmission. Likewise, for US OFDM modulated signals and OCDM coded signals are passed across the ODN to detect signal at OLT side via de-multiplexers (DEMUXs) [15].

Fig. 1(b) illustrates an integrated TWDM/OFDM PON where both OLT &ONUs incorporates four pairs of transmitters as well as receivers. It incorporates 4-QAM scheme with number of samples of 32768 & 2.5×10^9 symbols/s symbol rate to realize the system. Four downlink (1596-1598.4 nm) and four uplink (1527- 1529.4 nm) wavelengths for TWDM/OFDM integrated strictly as per ITU-T standard having 0.8 nm channel spacing. A single downlink Tx section illustrates random binary sequences generator at 40 Gbps traffic rate to be forwarded to a 4-QAM sequence generator at OLT side. After this, QAM signal is modulated at fast Fourier transform points of 512, 1024 and 64 cyclic prefix points. In-phase (I) & quadrature (Q) signals are filtered via the roll-off filters (roll-off factor = 0.2) for I/Q components modulation. Here, I/Q modulator includes an incoming continuous wave (CW) laser signal (0.15 MHz line width, -6 dBm input power), a couple of electrical gain after each filter and a pair of mach-Zehnder modulators (MZMs). After combining by a 2:1 power combiner the combined I/Q optical modulator outputs is passed through fiber-FSO link. Moreover, TWDM/OFDM beams in downlink direction are multiplexed viaa 4:1 AWG MUX at distinct wavelengths as well as transmitted over fiber-FSO link [15].

As depicted in Fig. 1(c), the incoming de-multiplexed signal is passed to two X couplers pairs (0.5 coupling) along with a local oscillator + phase shifter (90^0) to receive coherent orthogonal signals. Two sets of twice PIN photo detectors (PDs) are used for coherent detection followed by corresponding pairs of electrical subtractor & electrical amplifier having gain of 20dB.Meanwhile, to fix fiber nonlinearities & noise, the incoming signals are forward to a digital signal processing module, a decision device& a sequence decoder. Also, to reconstruct and correctly receive the QAM symbols meeting demodulator measures modulator at Tx. Again, to recover the Tx bit sequence, a QAM sequence detector identify the binary sequences along with de-mapped the electrical signal. Here, for generating VLC signals the incoming electrical signal is merged with DC bias signal (voltage = 4V) employing a bias tee to drive a red light emitting diode (LED) (65% quantum efficiency, 625 nm wavelength at 1 GHz) at 40 Gbps non-return to zero data rate. Moreover, a VLC signal is detected and analysed by using a bit error rate (BER) analyser [15].

Likewise, for uplink transmission in an integrated TWDM-OFDM using VLC, four input signals (1527-1529.4nm) generated via different laser diodes as realized in Fig. 1(b). It is followed by a time switch combined structure comprising two consecutive dynamic select Y generating uplink signals with specific duration to be forwarded to an OFDM modulator. After demodulation from OFDM demodulator at OLT side, a buffer selector incorporates to select the last iteration.

Fig. 1(d) illustrates the downlink transmission section of WDM-OCDM integrated system employing 2D-MFRS code showing three different Tx/Rx pairs for each coded users. For realizing downlink Tx section of WDM-OCDM, six lasers producing 1575-1579 nm wavelengths fed into a 6:1 AWG MUX followed by a 1:3 Fork. Also, each Tx section consists of a 1×6 AWG DEMUX illustrating six optical signals. After this, the AWG DEMUX output signals are transferred to a Subsystem 1 to 6. Here, each single Subsystem comprises of a bit sequence generator modulated via a MZM modulator and the obtained modulated signal is fed into a pair of consecutive fiber Bragg grading (FBG). After multiplexing from 6×1 AWG MUX the signal is passed through Subsystems followed by encoder. An encoder incorporates a 1×6 WDM DEMUX, 6×1 WDM MUX and MZM modulator modulate with non-return bit sequence generator at transmission speed of 40 Gbps to pass the data via a bidirectional fiber-FSO link. A decoder component is followed by photo detector, filter as well as a BER analyzer.

Fig. 1(e) illustrates US Tx section of WDM-OCDM using 2D-MFRS code for six US wavelengths (1260, 1260.8, 1261.6, 1262.4, 1263.2 and 1264 nm) generated by six laser diodes. Similar to the DS Tx WDM-OCDM section, the generated input signals passed through a 1×3 Fork and three Tx_US sections. Two dynamic select Y components produce signals at distinct time slots. Encoder section utilizes two FBGs, MZM and PRBS-NRZ. To improve the no. of subscribers, to reduce the phase induced intensity noise (PIIN) as well as to minimize the multiple access interference noise, several approaches of the two dimensional (2D) code design (spectral/spatial, time/spectral) can be realized. 2D-MFRS code comprises exiting one dimensional-FRS code in spectral domain together with spatial encoding [16]. Fig. 1(f) illustrates schematic diagram of 20 ONUs per RN in the system.

2.1. D-MFRS code

Assume $P = [p_1, p_2, p_3 \dots p_N]$ and $Q = [q_1, q_2, q_3 \dots q_N]$ code sequences of FRS having code

weight w_1 (code size=N_1) as well as w_2 (code size=N_2) considerably. Again, N_1&N_2 are number of end subscribers in spatial-spectral domains. While, $L_1 = N_1(w_1 - 2) + w_1$ as well as $L_2 = N_2(w_2 - 2) + w_2$ are code lengths of P and Q code sequences. 2D-MFRS code, $C_{g,h}$ is realized in terms of$c_{i,j}$ where $i\epsilon[0,1 \dots L_2 - 1]$ as well as $j\epsilon[0,1 \dots L_1 - 1]$. where S, code size and L, code length in $C_{g,h}$ can be defined as [17]:

$$C_{g,h} = \begin{bmatrix} c_{0,0} & c_{0,1} & c_{0,L_1-1} \\ c_{1,0} & c_{1,1} & c_{1,L_1-1} \\ \cdot & \cdot & \cdot \\ \cdot & \cdot & \cdot \\ \cdot & \cdot & \cdot \\ c_{L_2-1,0} & c_{L_2-1,1} & c_{L_2-1,L_1-1} \end{bmatrix} \quad (1)$$

Besides, 2D-MFRS code‘s cross correlation between $C^{(p)}$ and $C_{g,h}$, $g\epsilon[0,1 \dots N_1 - 1]$ and $h\epsilon[0,1 \dots N_2 - 1]$is expressed as [17]:

$$Y_{g,h}^{(p)} = \sum_{i=0}^{L_2-1} \sum_{j=0}^{L_1-1} {c_{i,j}}^{(p)} \times c_{i,j}(g,h) \quad (2)$$

where $C^{(p)}$ means characteristic matrix with $p\epsilon[0,1 \dots n - 1]$, n means no. of characteristic matrices, ${c_{i,j}}^{(p)}$ represents $(i,j)_{th}$ of $C^{(p)}$ and $c_{i,j}(g,h)$ is $(i,j)_{th}$ of $C_{g,h}$. The signal to noise ratio of the is measured as [17]:

$$SNR = \frac{(RP_r w)}{\frac{BL}{\Delta\vartheta}(I_{PD1} - I_{PD2})^2 + 2eB(I_{PD1} + I_{PD2}) + \frac{4KTB}{R}} \quad (3)$$

where R means load resistance, P_r means received power, $w$means code weight, B indicates electrical bandwidth, Lindicates code length, $\Delta\vartheta$ is optical bandwidth, I_{PD1} and I_{PD2} indicate received currents at two detectors at receiver, e is electric charge, K means Boltzmann constant, T is temperature.

Fig. 1(f) depicts the architecture of proposed wheel-based architecture supports 20 ONUs per remote node. Here, each 1:8 power splitter can serve maximum eight number of ONUs out of which few are active (on) and others are idle (off). As with the increase in ONUs, the system performance decays because of addition of multiple access interference, beat noise, shot and thermal noise. However, the design using higher number of ONUs contributes to scalability and efficiency in healthcare services enhance as more number of end users services can be handled simultaneously using scalable wired-wireless integrated link. Besides, the utilization of cost-effective red LED base VLC at end user side reduces the overall system cost at each ONU. Therefore, this design contributes to scalability and efficiency in healthcare services. Table 1 exhibits the several design parameters of proposed architecture.

Again, the Rx sensitivity is exhibited, as the minimum signal power required at the receiver terminals that provides the mandatory signal-to-noise rate at the detector. In the proposed work, BER of $\leq 10^{-9}$ is considered as criterion for maintaining minimum receiver sensitivity over hybrid fiber-FSO-VLC links. Mathematically, for the system, the receiver sensitivity (RS) is calculated as [18]:

$$Rs(dBm) = Receiversensitivity(dB) - \{IL + Powerpenalty\} > 32.5dB \quad (4)$$

where reference RS and power penalty is taken as -25 dB and 2 dB respectively, while insertion loss, IL for both DN and UP transmission having insertion losses at splitter, MUX, circulator and DEMUX, is given as [18]:

$$IL(dB) = IL_{Splitter} + IL_{MUX} + IL_{Circulator} + IL_{DEMUX} \quad (5)$$

After considering the values of different IL, total loss can be calculated as:

$$IL(dB) = 2 + 3 + 1 + 3 = 12dB \quad (6)$$

Therefore, minimum RS for the system using hybrid fiber-FSO-VLC links for various number of ONUs is calculated as:

$$Rs(dBm) = -25 - \{12 + 2\} > 32.5dB = -39dBm \quad (7)$$

Consequently, hybrid fiber–FSO–VLC link combinations are taken into consideration when determining the system's minimum necessary RS. This computation is carried out for various Optical Network Unit (ONU) counts. It sheds light on how well a system performs in different network settings.

Table 1. Design parameters [19-22]

Parameter	Value
VLC Range	20 m
FSO link loss	1 dB/km
Geometric loss	Yes
FSO range	3100 m
Attenuation	0.35 (air), 4.2 (fog), 6.2 (rain), 38.6 (snow) dB/km
Turbulence	10^{-17} -10^{-13} (weak to strong) $m^{-2/3}$
Aperture diameter	20 cm
Fiber length	100 km
Attenuation	0.2 dB/km
Dispersion	16.75 $ps.nm^{-1}.km^{-1}$
Dispersion slope	0.075 $ps.nm^{-2}.km^{-1}$
Splitter insertion loss	2 dB
Circulator insertion loss	1
Bandwidth	4 GHz
MUX/DEMUX Insertion loss	3 dB
Filter order	4
AWG Insertion loss	2 dB

Fig. 2 depicts the proposed work flow diagram.

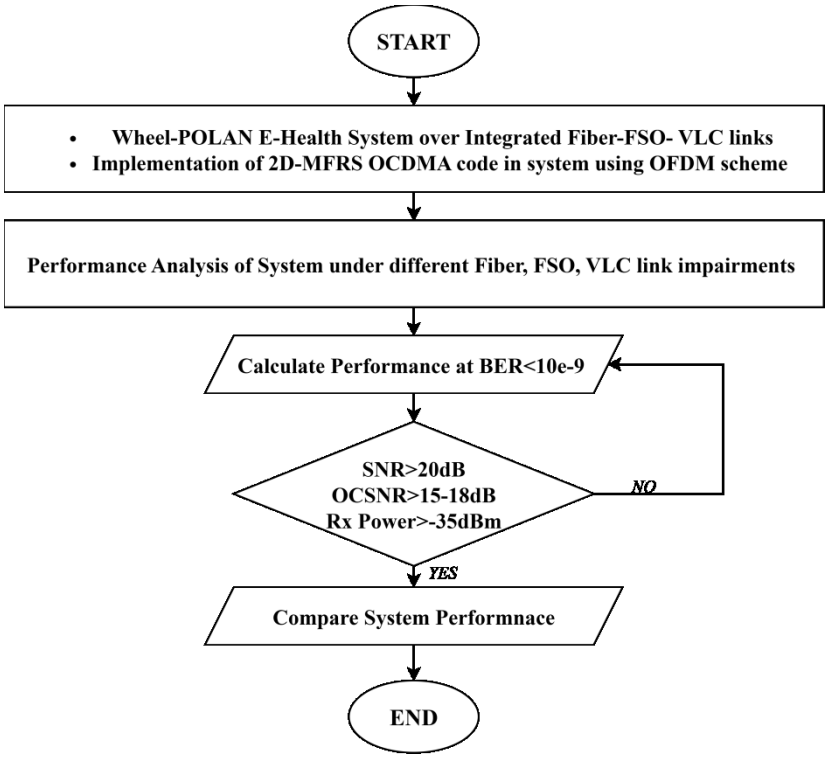

Fig. 2. Flow diagram of the proposed work

3. Results and discussion

Proposed architecture analysed using OptiSystem. The received FSO power, P_{re} under distinct climate conditions can be defined as [19–22]:

$$P_{re} = P_{tr}.\left(\frac{A_{eff}}{(\theta L)^2}\right).exp\left(-\delta L_{fso}\right) \tag{8}$$

whereP_{tr} means transmitted power. A_{eff} means antenna effective aperture area at Rx, θ means beam divergence, L is transmission distance and δ means attenuation coefficient depending on snow atmospheric conditions. Rain attenuation coefficient, δ_{rain} is expressed as [19–22]:

$$\delta_{rain} = \alpha R^t \tag{9}$$

where R means rain rate, α illustrates operating frequency coefficient, t illustrates temperature coefficient. Further, to evaluate the fog attenuation, both Kruse and Kim models are utilized as [19–22]:

$$\delta_{fog} = \frac{\frac{3.91}{V}\left(\frac{\lambda}{550}\right)^{-s}}{0.22} \tag{10}$$

where V illustrates visibility range, λ illustrates operating wavelength, s illustrates scattering size distribution coefficient which is defined as (Kruse model) [19–22]:

$$s = \begin{cases} 1.6 & V > 50km \\ 1.3 & 6 < V < 50km \\ 0.585V^{1/3} & V < 6km \end{cases} \tag{11}$$

Also, as per Kim's model [19–22]:

$$p = \begin{cases} 1.6 & V > 50km \\ 1.3 & 6 < V < 50km \\ 0.16V + 1.344 & 1 < V < 6km \\ V - 0.5 & 0.5 < V < 1km \\ 0 & V < 0.5km \end{cases} \tag{12}$$

Meanwhile, snow attenuation is defined as [23]:

$$\delta_{snow} = 58V^{-1} \tag{13}$$

In FSO the atmospheric turbulence effects introduce amplitude and phase variation of the propagating light, which causes fading as well as pulse abnormality. The strength of atmospheric turbulence as respects refraction structure parameter, C_n^2 is measured as [19–22]:

$$C_n^2 = (79 \times 10^{-6}.AX^{-2})^2 C_T^2 \tag{14}$$

where A exhibits atmospheric pressure, X is average temperature and C_T^2 is temperature structure parameter. Gamma-Gamma (GG) FSO distribution model generally used to realize the system performance because of its superb fitness over wide range turbulent effects from weak to strong as compared to others models. Therefore,

proposed architecture having GG channel distribution in FSO link is defined as:

$$f_{c_a}(c_a) = \frac{2(jk)^{\left(\frac{j+k}{2}\right)}}{\Gamma(j)\Gamma(k)} . h_a^{\left(\frac{j+k}{2}\right)-1} H_{j-k}\left[2(jkc_a)^{\frac{1}{2}}\right] \quad (15)$$

where $\Gamma(\cdot)$ is Gamma function, H_{j-k} is modified Bessel function, $(j-k)$ is Bessel function order, j and k are number of large & small scale irradiance fluctuations (effective eddies) are described as:

$$j = 1/e^{\left[(0.49k_0^2).\left(1+0.18d^2+0.56k_0^{\frac{12}{5}}\right)^{-7/6}\right]-1} \quad (16)$$

and

$$k = 1/e^{\left[\frac{0.51k_0^2\left(1+0.18d^2+0.56k_0^{\frac{12}{5}}\right)^{\frac{-5}{6}}}{\left(1+0.90d^2+0.62d^2k_0^{\frac{12}{5}}\right)^{\frac{5}{6}}}\right]-1} \quad (17)$$

Is aperture-averaged of atmospheric fading strength. Furthermore, mathematically, BER of the proposed design concerning FSO GG fading model and m-QAM OFDM-VLC is evaluated as:

$$BER = \frac{2}{log_2(m)}\left(1-\frac{1}{\sqrt{m}}\right) erfc\left(\sqrt{\frac{3}{2(m-1)}\times\frac{1}{EVM^2}}\right) + \frac{1}{2}\int_0^{\infty} f_{c_a}(c_a)\, erfc\left(\frac{\langle SNR\rangle s}{2\sqrt{2}\langle i_s\rangle}\right) ds \quad (18)$$

where $erfc(.)$ depicts complementary error function, m is level of modulation format, EVM means error vector magnitude, h_a means atmospheric turbulence, $\langle SNR\rangle$ mean signal to noise ratio, s is signal strength and i_s is signal current at photo-detector.

Fig. 3(a) and 3(b) exhibit the measured BER performance with distinct received optical power (ROP), for back to back (B2B), DS and US at 100 and 500 m FSO range respectively.

The performance is measured over fixed 10 m VLC range at 40/40 Gbps throughput. Receiver sensitivities of -17 dBm for US at 50 km and -16 dBm for US at 100 km is obtained at 100 m FSO range, at -9 log(BER) limit as depicted in Fig. 3(a). Also, the receiver sensitivities of -14 dBm for DS at 50 km and -13 dBm for DS at 100 km at 500 m FSO range is achieved. Moreover, sensitivities of -16 dBm for US at 50 km and -14 dBm for US at 100 km is achieved at 100 m FSO range. Similarly, -13 dBm and -12 dBm receiver sensitivity for DS at 50 km and DS at 100 km fiber length with 500 m FSO range is achieved. Acceptable power penalties of 1dB (power budgets=-27 dBm) over 100 m FSO and 2 dB (power budgets=-26 dBm) over 500 m FSO range are obtained. Additionally, diverse channels performance is again developed with the corroboration of eye patterns attained for B2B, US & DS over 50 and 100 km fiber length is depicted in Fig. 3(a) and 3(b). It is analysed that eye diagram at 100 km fiber with 100 m FSO link shows better performance compared with 100 km fiber with 500 m FSO in US followed by DS.

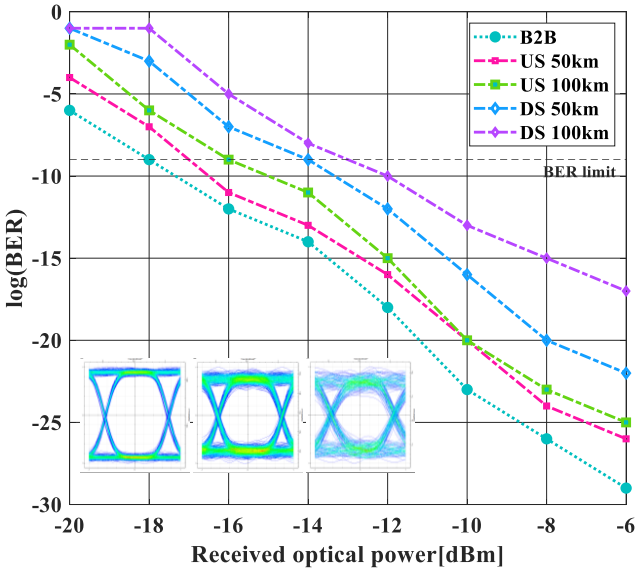

(a)

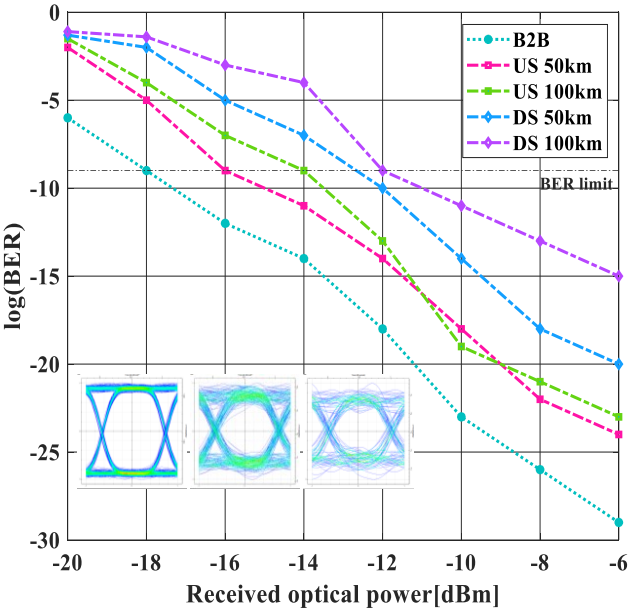

(b)

Fig. 3. System BER for DS and US channels at B2B, 50 km and 100 km fiber length at (a) 100 m and (b) 500 m FSO range. Insets: corresponding eye diagrams (colour online)

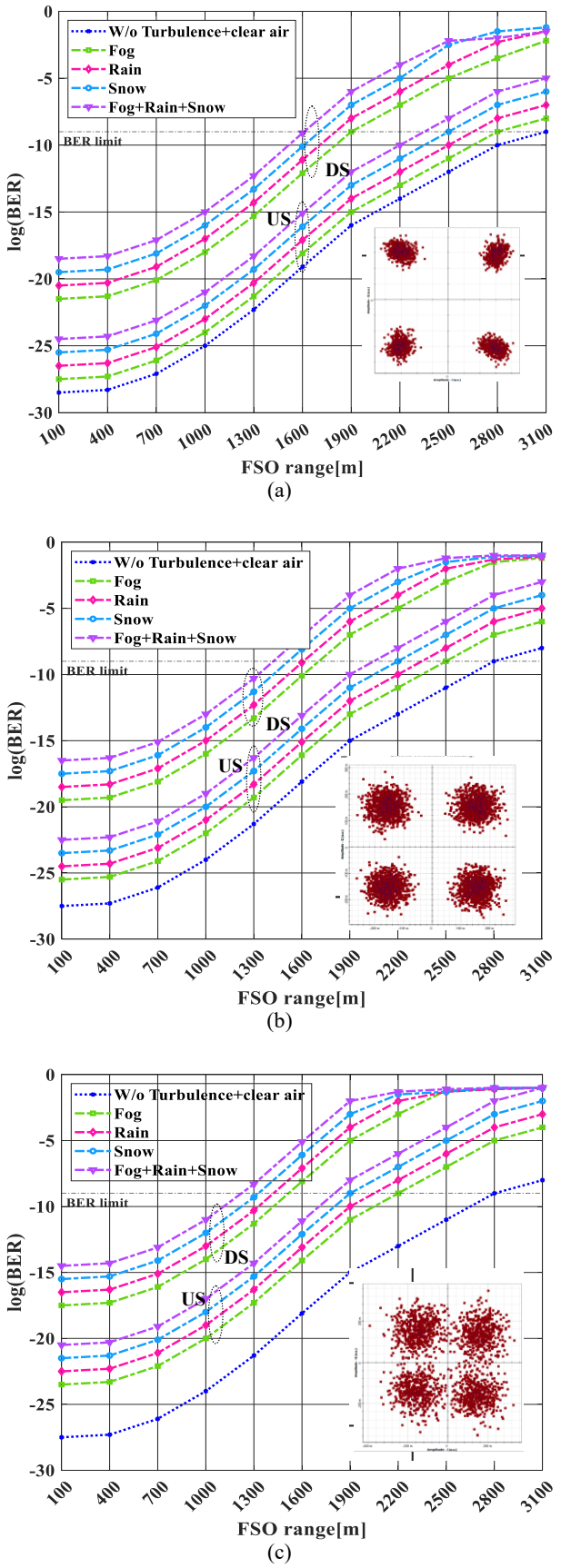

Fig. 4. Measured BER for varied FSO range concerning diverse weather conditions under (a) weak, (b) medium and (c) strong turbulent conditions. Insets: Constellation diagrams for US transmission at 3100 m (colour online)

Fig. 4(a), 4(b) and 4(c) indicate the log(BER) vs. FSO reach diagrams for full-duplex transmission under weather weak (10^{-17} $m^{-2/3}$), moderate (10^{-14} $m^{-2/3}$) and strong (10^{-13} $m^{-2/3}$) turbulence, respectively. Different weather conditions like clear air, fog, snow and fog+rain+snow are incorported for all turbulent condition while retaining the fiber span of 50 km and VLC span of 10 m at 40 Gbps/channel rate. It is delineated that by increasing the FSO range in the system, the effect of turbulence as well as weather scenarios on FSO becomes quite prominent leading to unsatisfactory BER.

Besides, for steady turbulent, BER analysis reprobates considerably as climate circumstances varies from without turbulence+clear air condition to clear air to snow unsurprisingly, particularly for worse weather scenario of fog+rain+snow. Meanwhile, with the increase in turbulence scenario from weak followed by moderate to strong, BER achievement again depreciates. It is owing to the motive that the inferior turbulence with climate effects insinuates larger channel inhomogeneity and consequently procures sufficient irradiance. The faithful FSO range of 3100 m can be achieved in the absence of turbulence under clear air condition. In a weak turbulent channel with fog, maximum FSO range of 2800 m.

Table 2 indicates the faithful FSO range attained under diverse atmospheric conditions as well as turbulent effects. It is sensed that optical signals transmission permits reliable FSO span best with fog followed by rain, snow and then fog+rain+snow under weak turbulence. Besides this, phase noise as well as frequency offset also conduces to misplaced points constellation diagrams causing worse modulation quality with more errors.

Table 3 revealed that wheel-hybrid PON/FSO/VLC incorporating 2D-MFRS surpasses other codes w.r.t. minor code weight, numerical subscribers, moderate complexity, allowable code length & required cross-correlation features. Table 4 defines that the bidirectional hybrid PON/FSO/VLC based on wheel topology provides high symmetric 10×100 Gbps throughput, 20 m VLC, 2800 m FSO and 130 km fiber length successfully with moderate maintenance cost than other systems. Table 5 illustrates the observed results of proposed system for different parameters.

Moreover, Ultra-high data rate transmission is made possible by the suggested fiber–FSO–VLC integrated connection. It uses sophisticated hybrid communication to reach 100 Gbps per channel. The technology combines FSO–VLC connections with single-mode fiber. High capacity and adaptable bandwidth across a range of distances are guaranteed by this integration that provide very good results along with enhanced quality matrices at the receiving end. It offers dependable and effective end-to-end connection. A symmetric throughput of 1 Tbps (10 × 100 Gbps) is provided by the bidirectional link. This performance is attained across a fiber distance of 130 km, 20 m VLC, and 2800 m FSO.

Table 2. Maximum FSO range for distinct atmospheric turbulent and climate conditions @log(BER)= -9

Climate	Faithful FSO span (m)					
	D/S	U/S	D/S	U/S	D/S	U/S
	Weak		Moderate		Strong	
Fog	1900	2800	1650	2500	1550	2200
Rain	1750	2650	1600	2350	1400	2150
Snow	1650	2500	1550	2200	1350	1900
Fog+Rain+Snow	1600	2350	1450	2150	1250	1850

Table 3. Comparison of various OCDMA codes

Ref.	Code weight	Code length	Complexity	Total users	Cross-correlation	Span (km)	Data rate
[24]	4	30	Medium	30	<1	20km	10Gbps
[25]	3	91	Medium	30	0	20km	0.622Gbps
[16]	4	30	High	30	≤1	-	0.622Gbps
[26]	4	2	High	52	<1	-	2.5Gbps
[17]	3	12	Medium	63	<1	40	32×1Gbps
(This work)	3	12	Medium	63	<1	100	2×10×100Gbps

Table 4. Comparison of various PON based designs based on topology

Ref.	Topology	Max. SMF range (km)	Wireless range (m)	VLC range (m)	No. of channels	Throughput /channel (Gbps)	Cost
[27]	Hybrid ring-tree	26	not used	-	not defined	1.25	High
[13]	Integrated ring-star	150	not used	-	not defined	15	Low
[28]	Ring	25	not defined	-	not defined	10	Low
[29]	Wheel	310	not used	-	8	50	Moderate
[30]	Ring	not defined	not used	-	not defined	10	Moderate
[31]	Hybrid ring-mesh	130	1900	-	10	10	High
[12]	Integrated ring-tree	100	not used	-	not defined	60	Moderate
[32]	Bus	0.1	500	-	3	10	Moderate
[33]	Bus	-	-	50	-	0.25	Low
This work	Wheel	100	2800 (FSO)	20	10	100	Moderate

Table 5. Observed results of the proposed system in an analyzer @ BER limit

Fiber distance (km)	Noise Figure (dB)	Gain (dB)	Input optical SNR (dB)	Output SNR (dB)	Output signal (dBm)
10	57.88	66.22	71.27	18.64	-81.35
30	60.31	63.88	71.99	18.58	-81.41
50	62.70	61.51	75.29	15.56	-84.43
70	65.05	59.10	75.23	15.33	-84.66
90	67.37	56.65	71.27	14.62	-85.37

4. Conclusion

An integrated PON system using OFDM-OCDM multiplexing over SMF-FSO-VLC link is realized. 2D-MFRS code is used for end-user connectivity. It is concluded that the system allows maximum fiber link distance of 100 km with front haul FSO and VLC range of 100 m and 20 m, respectively. At 10e-9 BER limit, FSO range over a downlink range of 1250-1900 m and 1850-2800 m in uplink direction under fog, rain, snow and weak-to-strong turbulence. It also provides acceptable power penalties of 1dB (power budgets = -27 dBm) over 100 m FSO and 2dB (power budgets = -26 dBm) over 500 m FSO range successfully. As compared to exiting codes, 2D-MFRS code offers better performance in terms of higher number of end-users with moderate complexity and limited code weight as well as code length. Meanwhile, it also shows better performance than existing design in terms of providing high data rate, link distance and low to moderate cost.

Looking ahead, the proposed architecture can be adopted in healthcare systems to offer high-capacity, radiation-free, and secure functionalities, applicable across indoor and outdoor hospital environments, and fostering medical research efforts aimed at improving human health.

References

[1] A. Ahad, M. Tahir, ECS Sensors Plus **2**, 011601 (2023).
[2] J. Rak, R. Girão-Silva, T. Gomes, G. Ellinas, B. Kantarci, M. Tornatore, Opt. Switch. Netw. **42**, 100619 (2021).
[3] Y. Cao, C. Gan, Optik **123**, 176 (2012).
[4] F. Hou, M. Yang, Optik **124**, 3824 (2013).
[5] Y.-K. Choi, M. Hanawa, X. Wang, C.-S. Park, J. Opt. Commun. Netw. **5**, 183 (2013).
[6] A. Amphawan, S. Chaudhary, T. K. Neo, M. Kakavand, M. Dabbagh, Wirel. Netw. **27**, 211 (2021).
[7] A. K. Garg, V. Janyani, B. Batagelj, N. H. Zainol Abidin, M. H. Abu Bakar, Opt. Fiber Technol. **61**, 102422 (2021).
[8] C. H. Yeh, C. W. Chow, C. S. Gu, B. S. Guo, Y. J. Cheng, J. H. Chen, Electron. Lett. **54**, 1228 (2018).
[9] S. B. Ahmad Anas, F. H. Hamat, S. Hitam, R. K. Z. Sahbudin, Photonic Netw. Commun. **23**, 33 (2012).
[10] Y. Gong, C. Gan, C. Wu, R. Wang, Telecommun. Syst. **57**, 327 (2014).
[11] P. Lafata, J. Vodrazka, Microw. Opt. **48**, 2611 (2006).
[12] S. Singh, S. Singh, Photonic Netw. Commun. **35**, 325 (2018).
[13] A. Bala, S. Dewra, Journal of Optical Communications **37**, 395 (2016).
[14] H. Emami, M. A. Balafar, Opt. Fiber Technol. **79**, 103341 (2023).
[15] C. H. Yeh, W. H. Hsu, B. Y. Wang, W. Y. You, J. R. Chen, C. W. Chow, S. K. Liaw, IEEE Access **8**, 189982 (2020).
[16] N. Jellali, M. Najjar, M. Ferchichi, H. Rezig, Opt. Fiber Technol. **36**, 26 (2017).
[17] H. Yousif Ahmed, M. Zeghid, W. A. Imtiaz, Y. Sharief, A. Sghaier, Optik **185**, 746 (2019).
[18] M. Kumari, Microw. Opt. Techn. Let. **65**, 1822 (2023).
[19] M. Kumari, S. K. Mishra, Photonics **11**, 355 (2024).
[20] M. Kumari, Wirel. Netw. **29**, 1721 (2023).
[21] M. Kumari, A. Sheetal, R. Sharma, Wireless Pers. Commun. **119**, 2539 (2021).
[22] M. Kumari, R. Sharma, A. Sheetal, T. Emerg. Telecommun. T. **32**, e4214 (2021).
[23] M. S. Awan, L. Csurgai-Horváth, S. S. Muhammad, E. Leitgeb, F. Nadeem, M. S. Khan, J. Commun. **4**, 533 (2009).
[24] T. H. Abd, S. A. Aljunid, H. A. Fadhil, Journal of Optical Communications **32**, 263 (2011).
[25] R. Matem, S. A. Aljunid, M. N. Junita, C. B. M. Rashidi, I. S. Ahmed, Optik **178**, 1051 (2019).
[26] R. A. Kadhim, H. A. Fadhil, S. A. Aljunid, M. S. Razalli, Opt. Commun. **329**, 28 (2014).
[27] C. Y. Li, C. H. Chang, Z. G. Lin, Photonics **8**, 515 (2021).
[28] C. H. Yeh, Y. R. Xie, C. M. Luo, C. W. Chow, IEEE Commun. Lett. **24**, 589 (2020).
[29] M. Kumari, J. Amb. Intel. Hum. Comp. **15**, 2439 (2024).
[30] Z. Tan, C. Yang, Z. Wang, J. Lightwave Technol. **35**, 4526 (2017).
[31] M. Kumari, Opt. Quant. Electron. **55**, 1098 (2023).
[32] M. Kumari, Internet Technology Letters **8**, e70023 (2025).
[33] H. Sun, L. Zhang, R. Jiang, X. Tang, IEEE Photonic. Tech. L. **37**, 609 (2025).

*Corresponding author: ichvivekmalik@gmail.com